JOURNAL OF SCIENCE AND ARTS

A STUDY OVER ELECTROCHEMICAL DEPOSITION OF NANOSTRUCTURES

ANDREEA STANCU[2], DORIN LEȚ[1]
[1]*Valahia University of Targoviste - Multidisciplinary S&T Research Institute, Dambovita*
[2]*Valahia University of Targoviste – Materials Science PhD School POS-DRU program, Dambovita*

Abstract: *This paper treats the problem of nanostructured materials manufactured through electrodeposition and electroless processes for industrial applications in order to demonstrate the vast richness promised by electrochemistry. The fundamental concern that dictate the control of the reaction rate and ensuing thickness and composition of the deposit is argued in relation to compositionally modulated nanolayers in a variety of architectures: core-shell nanoparticles, nanowires, pillars, tubes, and composite materials. The electrochemical processing technique is, in some cases, an alternative to other techniques like chemical vapor-deposition CVD methods, but it also finds an exclusive niche for the deposition of nanostructured materials of high aspect ratio geometries.*

Keywords: electrochemical deposition, nanomaterials, MCM system

1. Introduction

The process of electrochemical deposition is old and had become an integrated technique for the fabrication of nanosize devices. Electrodeposition, electroless deposition, and displacement reactions can be used to deposit metals, alloys, and metal-matrix composite materials, governed by electrochemical reactions. Nanomaterials prepared by electrodeposition are differentiated by at least one dimension in the nanometer range, they include nanostrutured thin-film multilayers, nanowires, nanowires with nanometric layers, nanotubes, nanosize particles embedded into metal matrices, and discrete or pressed nanoparticles with metal shells. Given the nanometric nature of the structures, the physical properties of nanomaterials can be considerably different from bulk materials having the same layout.

Electrochemical deposition consists in the reduction of metal ions with an impressed current or potential. On the other hand, electroless and displacement processes occur without an impressed current. Magnetic compositionally modulated multilayered thin films and nanowires are typical examples of electrodeposited nanostructured materials, while coatings around nanoparticles and lining nanoporous walls have been carried out by displacement and electroless processes. Electrochemical deposition had become known not only as a cost-effective alternative to vapor-deposition methods for thin films, but also as preferred method to deposit nanostructured layers onto irregular substrates and into deep indentations, allowing the fabrication of materials such as nanotubes and nanowires.

2. Multilayers compositionally modulated

Multilayer compositionally modulated MCM materials are synthesized by deposition, in a sandwich-like manner, of alternate layers having different compositions. One of the first examples of MCMs was demonstrated by Blum in 1921, when alternate Cu and Ni layers, tens of microns thick, were deposited from two different electrolytes. The resulting Cu/Ni multilayer improved the tensile strength of the electrodeposit compared to elemental copper deposits. Today, MCM materials of interest in other systems include not only mechanical properties (e.g., fracture and tensile strength, hardness) but also magnetic properties. Magnetic multilayers separated by paramagnetic layers on the nanoscale give rise to giant

magnetoresistance GMR, characterized by a decrease in resistance (>1%) with an applied magnetic field, as the magnetic domains change from an anti-ferromagnetic alignment to one that is in the direction of the magnetic field. Cobalt—copper, multilayer, Co/Cu, is one example that has been thoroughly examined in literature, both in the form of a thin film and nanowire. Figure 1 shows the MR response of an electrodeposited Co/Cu multilayer film with 1000 repeat bilayers, deposited from a pH 3 electrolyte containing 0.005*M* $CuSO_4$, 0.5M $CoSO_4$, and 0.54*M* boric acid. The copper was deposited with a low-current density of — 0.2mA/cm^2 and the cobalt at a high-current density of 20mA/cm^2, under quiescent conditions.

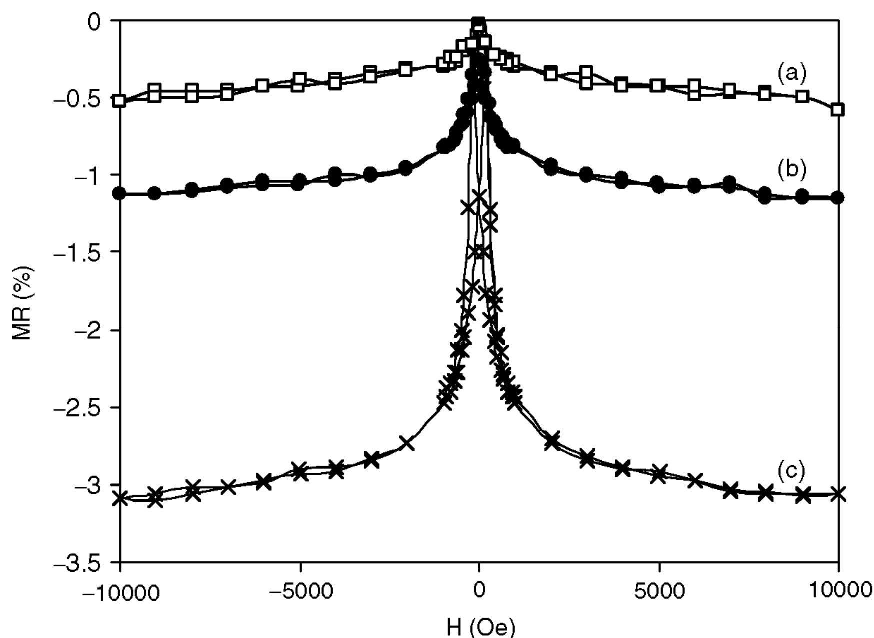

Figure 1. Co/Cu multilayers with 1000 bilayers, deposited on Si (111), with 2.5 nm Co layer thickness and variable Cu layer thicknesses: (a) 1 nm, (b) 1.5 nm, (c) 2 nm.

Resistance decrease is dependent upon a diversity of factors, including the choice of electrolyte, bilayer number and layer sizes, as represented in Figure 1. Higher room temperature GMR-percentage changes have been reported with thinner electrodeposited films having less than 100 bilayers, although the values are still 2—4 times lower than vapor-deposited counterparts.

Multilayer electrochemical deposition can be carried out using a single or dual bath approach. Dual-bath electrodeposition requires that either the substrate or electrolyte be transferred during the deposition of each layer. To simplify the process, a single bath is more desirable and the compositional modulation of the layers to be obtained by current pulsing.

In Figure 2 the steady-state partial current densities are represented for two depositing metals, M_1 and M_2 at the working electrode from a single electrolyte. The total polarization is shown as the dotted line. At point A, the reduction of M_1 occurs. At more negative potentials, such as at point B, both M_1 and M_2 deposit simultaneously. At point B, the rate of deposition of M_2 is larger than that of M_1, as a result of which the deposit is rich in the second component. In order to obtain layers with the highest purity, it is desirable for the rate of deposition of M_1 to be as small as possible, while depositing the M_2-rich layer. The trade-off, however, is that the low M_1 rate extends the processing time. Either the potential or current can be modulated in a square-wave pulse to fabricate the multilayers. Scanning tunneling microscopy of cleaved cross-sections of lead-thallium-oxygen nanometer size deposits showed that potentiostatic pulses resulted in more discrete layers than galvanostatic pulses.

In order to limit the reaction rate of the more noble species, its concentration in the electrolyte is maintained at a value that is orders of magnitude lower than the other metal ion

species. In the example given in Figure 1, the electrolyte composition of Cu(II), M_1, is 100 times lower than Co(II), M_2, which permits a layered deposit when the current is pulsed. Thus, at point B, the reaction rate of M_1 reaches a mass-transport-limiting current density, i_{lim}. At steady state, an estimate of the limiting current density can be readily determined, assuming that diffusion is the dominant mode of transport with a Nernstian boundary layer approximation,

$$i = i_{\mathrm{lim}} = \frac{-nFDC^b}{\delta} \quad (1)$$

where D (cm^2/sec) is the diffusion coefficient of the reacting species, C^b (mol/cm^3) its bulk concentration, δ (cm) the mass transport boundary layer thickness, n (equiv/mol) the number of electrons transferred, fixed by the reaction under consideration, and F (As/equiv) the Faraday's constant (96485 C/equiv). The boundary layer thickness is the most difficult to determine as it is dependent on the hydrodynamic environment surrounding the electrode. It is typically several hundred microns, while it has only tens of microns in well-mixed electrolytes.

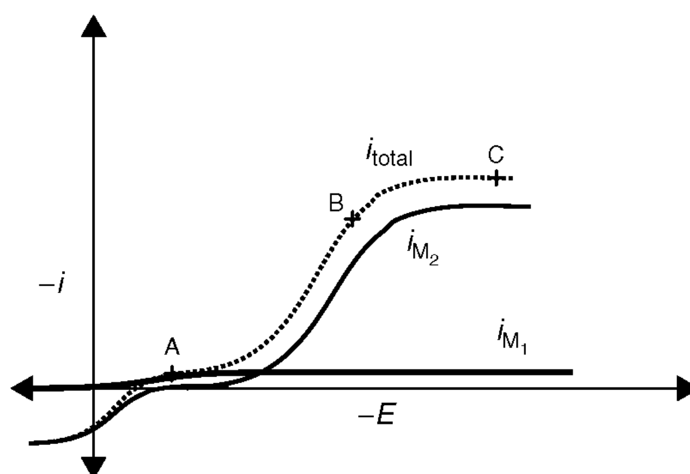

Figure 2 - Two electrodepositing metals with disparate reaction rates.

M_2, the less noble reactant, is in excess in the electrolyte, and generally deposits under kinetic control during multilayer fabrication. Deposition far from equilibrium can be approximated by a Tafel equation:

$$i = -i_0 \exp\left(\frac{-\alpha_c F}{RT}\eta_s\right) \quad (2)$$

this requires knowledge of two kinetic parameters, the exchange-current density, i_0 (A/cm^2) and the cathodic-transfer coefficient, α_c- (dimensionless). These values have been reported for a wide variety of reactions; however, i_0 is dependent on the species' activity, i.e. concentration, and is highly specific to a particular electrolyte. The surface overpotential, η_s- (V), is the polarization away from the equilibrium potential, when no concentration gradients occur. If the polarization is large, kinetic control of the M_2 reaction gives way to a transport control as described by Equation 1, and depicted at point C in Figure 2. Deposition, however, is not desirable at this region because of the loss in efficiency; both species are dominant by mass transport, due to the development of rough-surface deposits and excess-side reactions from the solvent.

The kinetic behavior is differentiated by a uniform concentration distribution of reactants near the electrode surface. During the multilayer fabrication, if the much noble species, M_1, is deposited below point A (Figure 2), under kinetic control, and then is co-deposited at point B, under mass transport control, there will be a change in the noble metal-concentration gradient that is time-dependent, resulting in a compositional gradient within the alloy layer. Classical descriptions of a single reacting species under a time-dependent diffusion control for a galvanostatic or potentiostatic pulse have been developed by Sands and Cottrell. Due to the enhanced compositional gradient of a reactant during pulsing, its limiting current is subsequently enhanced during the pulse. An expression for the larger pulse limiting current density, i_p, compared with the DC, unpulsed, counterpart (Equation 1) for a galvanostatic pulse,

$$i = i_{\mathrm{p}} = i_{\mathrm{lim}}\left(1-\frac{8}{\pi^2}\left(\frac{r-1}{r}\right)\sum_{k=1}^{\infty}\frac{1}{2(k-1)^2}\,\frac{\exp[(2k-1)^2 a\theta_2]-1}{\exp[(2k-1)^2 a\theta]-1}\right)^{-1} \tag{3}$$

where r is the ratio of the first current-density pulse (point A, Figure 2) to the second value (point B, Figure 2), a ($=\pi^2 D/4\delta^2$) the diffusion parameter, the second period duration, and θ the cycle time. Equation (3) predicts that for the CoCu/Cu system, the amount of Cu co-deposited with Co in the alloy layer of a multilayer will be larger than Cu co-deposited with Co as a DC plated bulk alloy.

A portion of the anodic component of the partial-current density from the less noble metal species is shown in the lower left-hand corner of Figure 2. Depending on the kinetics of this reaction, there can be a simultaneous displacement of M_2 deposited metal by the more noble species, M_1, occurring at the start of the M_1 pulse during multi-layer electrodeposition. The displacement for the CoCu/Cu system:

$$\mathrm{Co(s)} \rightarrow \mathrm{Co(II)} + 2e^- \tag{4}$$

$$\mathrm{Cu(II)} + 2e^- \rightarrow \mathrm{Cu(s)} \tag{5}$$

is controlled, so that even when the impressed current is cathodic (negative), there can still be a small anodic contribution, given by the following general expression:

$$i = i_0 \exp\left(\frac{\alpha_{\mathrm{a}} F}{RT}\eta_{\mathrm{s}}\right) \tag{6}$$

where α_a is the anodic transfer coefficient. The outcome of displacement reactions occurring during the processing of the multilayer not only results in a change in the composition, but can also exaggerate the concentration gradients at the layer interfaces. To suppress displacement reactions, strategies such as adding additives to alter the kinetic parameters in Equation 6 or alloying the magnetic layer with a corrosion resistance material can be considered. Larger GMR values were observed with a small amount of Ni incorporated into the Co-alloy layer as shown in Figure 3.

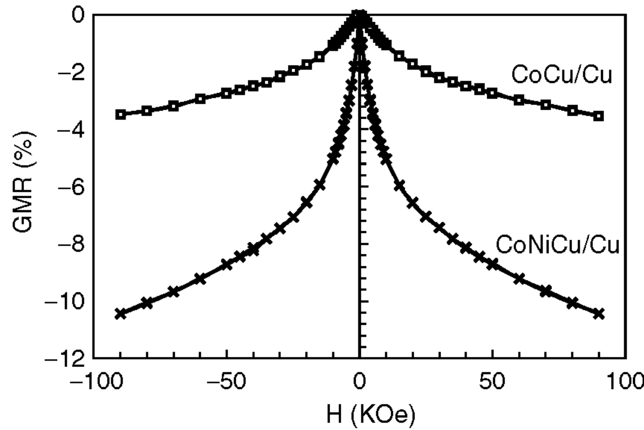

Figure 3. Giant magnetoresistance of two comparable electrodeposited multilayer films with one film containing 3.5 wt% Ni in the Co alloy layers, with 2000 bilayers

The partial-current density Equations 1, 3 and 6 are vitally important to the design and prediction of the layer at composition, *x*,

$$x_j = \frac{i_j/n_jF}{\sum_k i_k/n_kF} \tag{7}$$

and thickness, Δ, in conjunction with Faraday's law, which relates the mass plated to the charge passed,

$$\Delta = \sum_j \frac{M_j i_j t}{n_j \rho_j F} \tag{8}$$

for species *j* with atomic weight *M*, density *ρ*, and time of deposition, *t*. In the case of electrolytes containing mixtures of iron group (Co, Ni, Fe) ions, the kinetic information should be ascertained from the alloy electrolyte rather than from elemental, single-metal deposition, on account of the anomalous-co-deposition behavior. Anomalous co-deposition refers to the preferential deposition of the less noble metal species, and has been widely reviewed with regard to bulk alloy electrodeposition.

3. Nanomaterials

3.1. Nanowires

To minimize concentration gradients within a multilayer, deposition into recessed geometries is inherently agreeable to improved electrodeposits. Template syntheses in nanoporous membranes are prepared in anodic-aluminum oxide, polycarbonate, and diblock-copolymer membranes. Nano dimensional layers within a nanowire are of particular interest for GMR studies when the current flow is perpendicular to the plane of the layers, referred to as CPP-GMR. In contrast, current-in-plane giant magnetoresistance CIP-GMR is the preferred mode of measurement for thin-film multilayers because of the extremely small values of resistance in the perpendicular direction, which precludes accurate and easy analysis. In CIP-GMR, the characteristic scaling length is the electron mean-free path, typically a few nanometers. However, for CPP-GMR, the critical length scale is the spin-diffusion length, which is generally larger than 10nm, and thus larger multilayer sizes can be tolerated.

In Figure 4 a transmission electron micrograph image of a CoNiFeCu/Cu nanowire is represented, showing multilayer's that are evident near the edge of a 200-nm diameter wire. The layer sizes of the Co-rich alloy and Cu layers are 4 and 2nm, respectively. The CPP-GMR of an array of nanowires is compared with a thin-film CIP-GMR with comparable layer sizes and chemical composition. While the GMR value is about the same, the magnetic field sensitivity clearly differs. Nanowires of multilayers have also been studied in literature for a variety of other systems. For example, room-temperature CPP-GMR of Co/Cu multilayer nanowires was reported to be 14-15% and 20%. The CoNi/Cu nanowires have been reported as possessing significantly larger GMR, 55% at room temperature.

These features render magnetic nanowires of interest for high-density magnetic recording. Earlier researches with Fe deposition into alumina-nanoporous templates also reported similar findings with an easy axis parallel to the wires with enhanced coercivity. Magnetic-alloy nanowires from CoFe, CoNi, NiFe, and CoNiFe have been reported as being not layered.

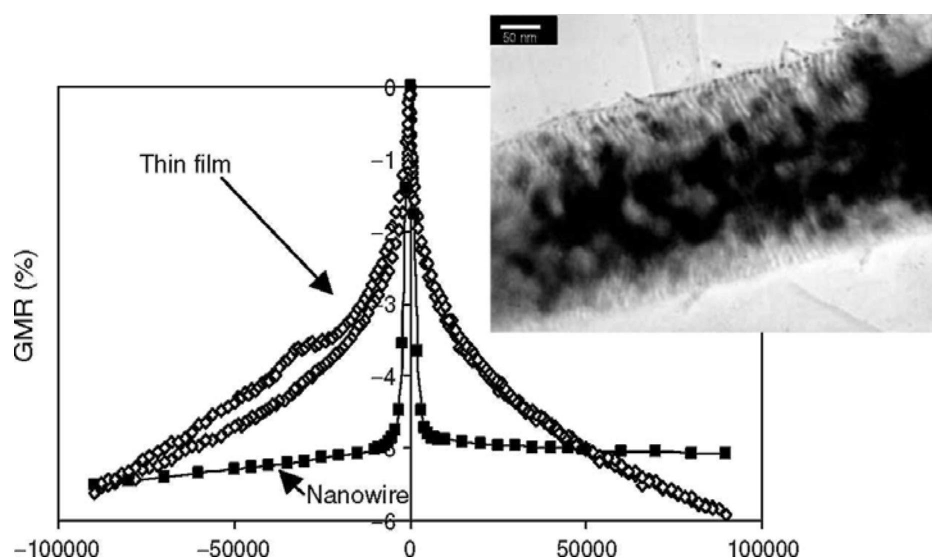

Figure 4. Thin film CPP-GMR and CIP-GMR of a CoNiFeCu/Cu 200nm nanowire

3.2. Nanotubes

They represent another type of nanoscale architecture fabricated inside nanoporous membranes for advanced catalytic and sensory materials. Electro-less deposition of metals inside the pores of membranes requires use of a chemical reducing agent to deposit the metal onto a surface from solution. A sensitizer which binds to the pore wall is usually used at the beginning. The sensitized surface is activated by exposure to a catalyst, resulting in the formation of discrete nanoscopic-catalyst particles. Finally, the catalyst-covered surface is immersed in the electrolyte containing the ions of the metal to be deposited and the reducing agent, for a surface-constrained deposition on the pore walls. Therefore, at the pore surface, the cathodic reaction (metal deposition) is equal to the anodic reaction (oxidation of the reducing agent) without any external power supply. Dissolution of the membrane can release an array of deposited tubes if needed. Nanowires can also be achieved in this fashion by immersing the nanoporous membrane for longer periods of time. Unlike electrochemical deposition, electro-less method provides no control over modulating the composition for alloy deposition. Also, the electro-less deposition cannot control the length of the nanowires or the nanotubes.

By knowing the rates of each reaction there can be determined the rate of electro-less deposition. Figure 5 schematically represents the partial current density of the cathode-deposition reaction ($M^{n+} + ne^- \rightarrow M$), and the anodic reaction of the reducing agent ($Red \rightarrow Ox + ne^-$). The equilibrium reduction/oxidation potential of the metal deposition, equilibrium

potential, E_1, must be more noble, thus larger, than the reducing agent equilibrium potential, E_2, thus $E_1 > E_2$. The schematic in Figure 5 is often referred to as an Evan's diagram, depicting the absolute value of the partial current density with potential in order to view both the anodic and cathodic reactions in the same quandrant of the graph. A logarithm scale is used for the current-density axis, since kinetic expressions are exponential in nature (i.e., Equations 2 and 6), and thus these regions will appear as potential-dependent straight lines. Potential-independent regions identify mass-transport control. The intersection of the two partial-current densities provides the resulting reaction rate, or current density of the electro-less process at a potential intermediate between the two equilibrium half-cell potentials. The Evan's diagram illustrates this concept of the "mixed-potential theory" where the resulting current density and potential of the electro-less process depends on the kinetics or transport limitations involved in both the "mixed" anodic and cathodic systems.
Pt and Ni tubes and wires electrodeposition has been observed in aluminum oxide membranes, the tube formation was a result of a nonuniform electric field concentrated at the pore wall. CoNiCu tubes were deposited from a boric acid electrolyte at a constant potential at efficiencies lower than 50%. An increase in the current efficiency, by a change in the electrolyte composition, resulted in the wire formation. Thus, gas-evolving side reactions in tube formation are suspected to be an additional controlling feature.

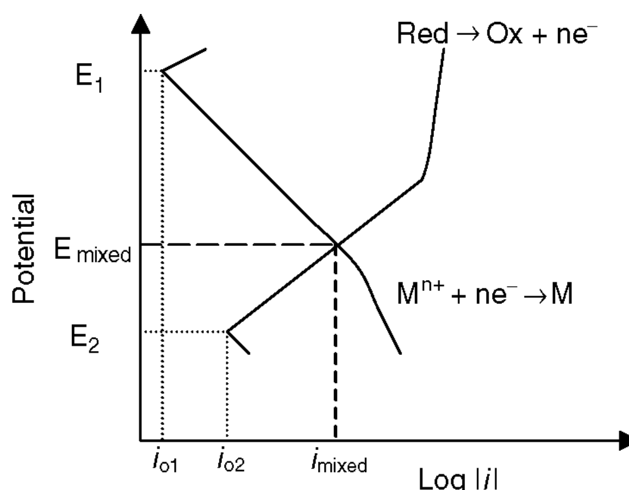

Figure 5. Schematic of the Evan's diagram showing the electroless process.

3.3. Pillars

The difficulty of measuring a single nanowire and the random array of the nanowires represents a disadvantage of nanowire deposition of multilayers. An alternative architecture is micro-size pillars that still render GMR to be measured in the CPP mode.

Using vapor-deposition techniques etching through thin films of multilayers, it had been shown in literature, that the fabrication of CPP-GMR pillars is possible. Optical lithography and reactive-ion-etching techniques are also used to fabricate pillars of vacuum-sputtered Fe/Cr multilayers, as well as molecular beam epitaxy evaporation deposition of Co/Cu multilayers. Over 50% CPP-GMR was observed and the researchers showed that the CPP-GMR mode measurements were often larger than measurements in the CIP mode.
Multilayered material electrodepostion into a lithographic pattern, rather than by etching it, can offer a cost-effective alternative. In addition, the deposition of materials into deep recesses is problematic with vapor deposition, line-of-sight type of techniques. The advantage of using electrodeposition for pillar fabrication is the same as for nanowire generation; it can offer conformal deposition in deep recesses.

On planar electrodes in unagitated electrolytes typical diffusion layer thicknesses are of the order of 100 Lim. Thus, electrodeposition into deep recesses >100 µm, will extend the

nonsteady-state regime for diffusion-controlled reactions, compared with planar electrodes. The convective hindrance of the recess further increases the diffusion boundary layer thickness by roughly the size of the recess depth. An estimate of the change of the limiting-current density with time of a species inside a recess, where the outside pore-mouth region of the recess is well mixed, is given in two limits.

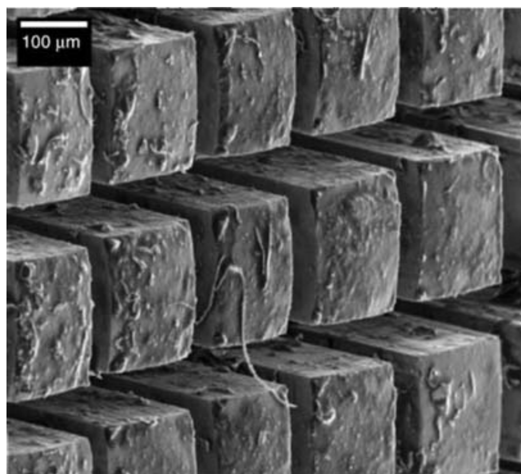

Figure 6. Array of CoCu microposts fabricated by x-ray lithography.

A short-time approximation for a reduction reaction follows

$$i = -nFc^b\left(\frac{D}{\pi t}\right)^{1/2}\left[1 + 2\exp\left\{\frac{-\pi^2 Dt}{L^2}\right\} + 2\exp\left\{\frac{-4\pi^2 Dt}{L^2}\right\} + \ldots\right] \tag{9}$$

where L is the recess depth. The leading term describes the Cottrell behavior on an unrecessed surface. At long times, the limiting current density is given as

$$i = \frac{-nFc^b D}{L}\left[1 + 2\exp\left\{\frac{-\pi^2 Dt}{L^2}\right\} + 2\exp\left\{\frac{-4\pi^2 Dt}{L^2}\right\} + \ldots\right] \tag{10}$$

and at steady state this reduces to Equation (1) where $\delta = L$.

From Equation 10 can be noticed that for typical metal ions, the time to achieve steady state in a recess hundreds of microns deep can be several seconds to minutes. During multilayer pulse plating, the diffusion-controlled species, often Cu, is depositing under a nonsteady regime at the start of deposition, during both the magnetic alloy deposition layer and the elemental Cu layers. As the deposition proceeds, the limiting-current density of the transport-controlled species will increase, due to a shortened boundary-layer thickness. In addition, the transient change in its concentration near the electrode surface is also altered so that steady state is achieved sooner. Regardless of how the deposition is controlled, galvanostatically or potentiostatically the consequence of this dynamic effect will result in more of the transport-controlled species in the second, magnetic layer.

4. Considerations

Fabrication of nanomaterials via electrochemical deposition is a wide area, and only a short overview has been presented in this study just to list the leading topics and challenges in this field. Emphasis has been placed on MCM systems area of industrial interest for a wide variety of applications. Compositionally modulated multilayer's, having nanosize dimensions, can be deposited as thin films, nanowires, pillars, and nanotubes and are governed by the

electrodeposition process. Compositional control of the process requires knowledge of the kinetic and mass-transport regions of the depositing metals. Nanoparticles used as discrete particles may rely on electro-less fabrication methods for the generation of shells around the nanoparticle core. Using template synthesis methods, such as alumina-porous membranes and track-etched polycarbonate porous membranes, to electrochemically deposit metal nanoparticles inside the pores has become popular in the recent years. These deposits have been studied in the context of a wide spectrum of scientific goals ranging from catalysis to magnetic properties and magnetic-data storage. Attention has also been focused on the application of small metal particles in surface-enhanced spectroscopy, photocatalysis and selective solar absorbers. Studies with atomic absorption have shown that iron, nickel, cobalt, and gold particles have equivalent areas per volume, with particle radii in the range 3 to 5 nm. Magnetic measurements on iron, nickel, and cobalt films reveal them to be highly anisotropic with magnetization perpendicular to the surface of the film. The unusual optical absorption of noble-metal nanoparticles such as copper, silver, and gold embedded in a dielectric medium such as alumina renders them of interest for optical applications.

References

[1] Weihnacht, V., Peter, L., Toth, J., Padar, J., Kerner, Z., Schneider, C.M., Bakonyi, I., *J. Electrochem. Soc.*, 150: C507-C515, 2003.

[2] Ohgai, T., Hoffer, X., Fabian, A., Gravier, L., Ansermet, J.P., *J. Mater. Chem.*, 13: 2530-2534, 2003.

[3] Chassaing, E., *J. Electrochem. Soc.*, 148: C690-C694, 2001.

[4] Kelly, J., Kern, P., Landolt, D., *J. Electrochem. Soc.*, 147: 3725-3729, 2000.

[5] Nabiyouni, G., Schwarzacher, W., Rolik, Z., Bakonyi, I., *J. Magn. Magn. Mater.*, 253: 77-85, 2002.

[6] Zhang, J., Moldovan, M., Young, D.P., Podlaha, E.J., *Proceedings of the 205th Meeting of the Electrochemical Society on Electrochemical Processing in ULSI and MEMS*, San Antonio, TX, 2004.

[7] Huang, Q., Podlaha, E.J., *J. Electrochem. Soc.*, 151: C119-C126, 2004.

[8] Khan, H.R., Petrikowski, K., *Mater. Sci. Eng*. C, 19: 345-348, 2002.

[9] Yoo, W.C., Lee, J.K., *Adv. Mater.*, 16: 1097-1101, 2004.

[10] Davis, D., Podlaha, E.J., *Electrochem. Solid-State Lett.*,8: D1-D4, 2005.

[11] Platt, M., Dryfe, R.A.W., Roberts, E.P.L., *Electrochim. Acta*, 49: 3937-3945 2004.

[12] Platt, M., Dryfe, R.A.W., Roberts, E.P.L., *Chem. Commn.*, 20: 2324-2325, 2002.

[13] Johans, C., Konturri, K., Schiffrin, D.J., *J. Electroanalyt. Chem.*, 526: 29-35 2002.

[14] B. Ravel, E.E. Carpenter, and V.G. Harris, *J. Appl. Phys.*, 91: 8195-8197, 2002.

[15] Lin, J., Zhou, W., Kumbhar, A., Wiemann, J., Fang, J., Carpenter, E.E., O'Connor, C.J., *J. Solid State Chem.*, 159: 26-31 (2001).

[16] W.L. Zhou, E.E. Carpenter, J. Lin, A. Kumbhar, J. Sims, and C.J. O'Connor, *Eur. Phys. J. D: At., Molecular Optical Phys.*, 16: 289-292, 2001.

[17] Carpenter, E.E., Sims, J.A.,Wienmann, J.A., Zhou, W.L., O'Connor, C.J., *J. Appl. Phys.*, 87: 5615-5617, 2000.

[18] Salazar-Alvarez, G., Mikhailova, M. Toprak, M., Zhang, Y., Muhammed, M., *Materials Research Society 2001 Fall Meeting Symposium Proceedings,* Vol. 707, 263-268, 2002.

[19] Son, S.U., Jang, Y., Park, J., Na, H.B., Park, H.M., Yun, H.J., Lee, J., Hyeon, T., *J. Am. Chem. Soc.*, 126: 5026-5027, 2004.

[20] Park, J.-I., Kim, M.G., Jun, Y.-W., Lee, J.S., Lee, W.-R., Cheon, J., *J. Am. Chem. Soc.*, 126: 9072-9078, 2004.

[21] Guo, Z., Kumar, C.S.S.R., Henry, L.L., Doomes, E.E., Hormes, J., Podlaha, E.J., *J. Electrochem. Soc.*, 152: D1-D5, 2005.

[22] Lozano-Morales, A., Podlaha, E.J., *J. Electrochem. Soc.,* 151: C478-C483, 2004.
[23] Panda, A., Podlaha, E.J., *Electrochem. Solid-State Lett.*, 6: C149-C152, 2003.
[24] Erler, F., Jakob, C., Romanus, H., Spiess, L., Wielage, B., Lampke, T., Steinhauser, S., *Electrochim. Acta*, 48: 3063-3070, 2003.
[25] Wang, T., Kelly, K., *J. Micromech. Microeng.*, 15: 81-90, 2005.

Manuscript received: 12.03.2009 / 02.05.2009